THE JOURNAL OF BIOLOGICAL CHEMISTRY VOL. 281, NO. 22, pp. 15337–15344, June 2, 2006

The Yeast Prion Ure2p Native-like Assemblies Are Toxic to Mammalian Cells Regardless of Their Aggregation State*[S]

Received for publication, October 27, 2005, and in revised form, March 9, 2006 Published, JBC Papers in Press, March 29, 2006, DOI 10.1074/jbc.M511647200

Laura Pieri[‡], Monica Bucciantini[‡], Daniele Nosi[§], Lucia Formigli[§], Jimmy Savistchenko[¶], Ronald Melki[¶1], and Massimo Stefani[‡‖2]

From the [‡]Department of Biochemical Sciences, [‖]Interuniversity Centre for the Study of the Molecular Basis of Neurodegenerative Diseases, and [§]Department of Anatomy, Histology, and Forensic Medicine, University of Florence, Florence 50134, Italy and [¶]Laboratoire d'Enzymologie et Biochimie Structurales, Centre National de la Recherche Scientifique, 91198 Gif-Sur-Yvette Cedex, France

The yeast prion Ure2p assembles *in vitro* into oligomers and fibrils retaining the α-helix content and binding properties of the soluble protein. Here we show that the different forms of Ure2p native-like assemblies (dimers, oligomers, and fibrils) are similarly toxic to murine H-END cells when added to the culture medium. Interestingly, the amyloid fibrils obtained by heat treatment of the toxic native-like fibrils appear harmless. Moreover, the Ure2p C-terminal domain, lacking the N-terminal segment necessary for aggregation but containing the glutathione binding site, is not cytotoxic. This finding strongly supports the idea that Ure2p toxicity depends on the structural properties of the flexible N-terminal prion domain and can therefore be considered as an inherent feature of the protein, unrelated to its aggregation state but rather associated with a basic toxic fold shared by all of the Ure2p native-like assemblies. Indeed, the latter are able to interact with the cell surface, leading to alteration of calcium homeostasis, membrane permeabilization, and oxidative stress, whereas the heat-treated amyloid fibrils do not. Our results support the idea of a general mechanism of toxicity of any protein/peptide aggregate endowed with structural features, making it able to interact with cell membranes and to destabilize them. This evidence extends the widely accepted view that the toxicity by protein aggregates is restricted to amyloid prefibrillar aggregates and provides new insights into the mechanism by which native-like oligomers compromise cell viability.

It is widely accepted that transmissible spongiform encephalopathies, a group of neurodegenerative diseases in mammals, are due to misfolding of the infectious prion protein (PrP)[3]; when altered, the protein is able to promote the conformational conversion of the normal cellular form PrP^{C} into the misfolded form PrP^{Sc} (1).

Prion proteins are also present in yeast cells. *Saccharomyces cerevisiae* contains at least four prion-like proteins, including Ure2p, which is found aggregated intracellularly under certain conditions. However, unlike mammalian prions, which display cytotoxicity in their aggregated form, Ure2p appears substantially noncytotoxic when aggregated into yeast cells (2), providing the molecular explanation for the change of phenotype given by the nonchromosomal genetic element [URE3] (3, 4). Such a change of phenotype could provide an evolutionary advantage to yeast cells by regulating nitrogen catabolism (5). When sources rich in nitrogen, such as ammonia, are available, Ure2p is believed to down-regulate the expression of gene products involved in the use of nitrogen-poor sources by binding the transcription activator Gln3p and preventing its migration into the nucleus (6). In wild-type cells, Ure2p is dispersed in the cytoplasm, whereas the [URE3] phenotype is caused by the appearance of an altered, self-propagating form of Ure2p ($Ure2p^{[URE3]}$) able to form in the cytoplasm large globular or elongated aggregates (4). This variant of Ure2p is inactive, resulting in the apparent loss-of-function phenotype.

Ure2p is a cytoplasmic homodimer, each monomer consisting of two domains: a highly flexible and poorly structured N-terminal domain (residues 1–93) rich in Gln and Asn (7, 8) and a compactly folded C-terminal domain (residues 94–354) rich in α-helices (9) whose crystal structure has been determined (10, 11). The C-terminal domain is the functional region, consisting of two subdomains and bearing similarity in sequence, fold, and substrate affinity to the glutathione *S*-transferase family proteins (12). Indeed, the C-terminal domain binds GSH with high affinity in a cleft running along the domain interface similarly to the active site of glutathione *S*-transferases (13).

The structural organization of the highly flexible, largely unstructured Ure2p N-terminal domain displays overall similarity to the corresponding domains found in mammalian prions (14). Since it has been shown that synthetic peptides encompassing the sequences of different regions of the N-terminal domain of PrP are able to aggregate into amyloid fibrils, it has been suggested that this region governs PrP fibrillization (15). Similarly, the N-terminal domain of Ure2p is of fundamental importance for aggregation; actually, overexpression of either Ure2p or its 65 N-terminal residues in yeast cells is sufficient to increase the spontaneous rate of [URE3] appearance by 1000-fold (4).

Under physiological conditions, Ure2p assembles *in vitro* into oligomers, eventually giving rise to fibrils similar to those observed in yeast cells carrying the [URE3] phenotype (7, 9). These fibrils share several morphological, structural, and tinctorial features with amyloids, including enhanced resistance to proteolysis (7, 9, 16), increased thioflavin-T fluorescence, and the yellow-green birefringence in cross-polarized light upon Congo red binding (17). However, these fibrils lack the classical x-ray diffraction pattern characteristic of amyloids, and their constituent monomers maintain the native structure rich in α-helices, can bind GSH (16, 18), and show gluta-

* This work was supported by Italian Ministero dell'Istruzione, dell'Università e della Ricerca Grants 2003054414 and RBNE01S29H_004 and the French Ministry of Education and Research through the Groupement d'Interêt Scientifique Prions. The costs of publication of this article were defrayed in part by the payment of page charges. This article must therefore be hereby marked "*advertisement*" in accordance with 18 U.S.C. Section 1734 solely to indicate this fact.

[S] The on-line version of this article (available at http://www.jbc.org) contains supplemental Fig. 1.

[1] To whom correspondence may be addressed. E-mail: melki@lebs.cnrs-gif.fr.

[2] To whom correspondence may be addressed: Dept. of Biochemical Sciences, University of Florence, Viale Morgagni 50, 50134 Florence, Italy. Tel.: 39-055-4598307; Fax: 39-055-4598905; E-mail: stefani@scibio.unifi.it.

[3] The abbreviations used are: PrP, prion protein; MTT, 3-(4,5-dimethylthiazol-2-yl)-2,5-diphenyltetrazolium bromide; ROS, reactive oxygen species; CM-H_2 DCFDA, 5-(and 6)-chloromethyl-2′,7′-dichlorodihydrofluorescein diacetate, acetyl ester.

thione peroxidase activity (19). Accordingly, these fibrils have been indicated as native-like. The presence of native-like monomers in these fibrils has led us to propose a model in which Ure2p assembly is driven by subtle conformational changes and nonnative inter- and/or intramolecular interactions (16, 18).

Upon incubation at 60 °C for 1 h, the native-like fibrillar aggregates undergo structural modifications and evolve into fibrils similar in appearance to the native-like fibrils when observed by electron microscopy; however, they lose the ability of the native-like fibrils and the soluble protein to bind GSH and to nucleate assembly. Moreover, they display a significant increase in β-sheet content, and their x-ray diffraction pattern is characteristic of amyloid fibrils (18).

An alternative model has been proposed for Ure2p assembly under conditions slightly different from those leading to the appearance of native-like fibrils. Under these conditions, the first 80 residues of the prion domain of each monomer stack to form an amyloid core rich in β structure. The latter is connected by the remaining portion of the N-terminal domain to the C-terminal domain that maintains substantially its native fold and surrounds the amyloid core (20, 21). In this case, inactivation of Ure2p upon fibril formation would be the consequence of a steric block of the native-like C-terminal domain (22).

Despite the wealth of studies on the morphological, physiological, and structural features of Ure2p and its aggregates, presently there is a substantial lack of information on the toxic effects of the latter on cultured cells. The availability of different conformational states (fibrillar, amyloid, fibrillar, native-like, oligomeric, native-like) of Ure2p prompted us to use such a protein as a model to investigate some molecular features of the toxicity of protein assemblies to cultured cells. Of course, our data cannot be directly extended to yeast cells, although they could be of importance for the cell biology of yeast prions. Therefore, the aim of this study was to investigate whether different types of Ure2p aggregates display cytotoxicity to mammalian cultured cells and to elucidate the biochemical features of cell injury (if any). Such an investigation was carried out using murine endothelioma H-END cells, previously shown to be highly affected by the exposure to prefibrillar amyloid aggregates of a disease-unrelated protein (23, 24). The use of H-END cells allowed us to compare the cytotoxic effects of native-like Ure2p aggregates with those described on the same cell type exposed to prefibrillar and fibrillar amyloid aggregates (23, 24).

EXPERIMENTAL PROCEDURES

Assembly of Ure2p into Oligomers and Fibrils—Full-length Ure2p (Ure2p 1–354) and its C-terminal region (Ure2p 94–354) were expressed in *Escherichia coli*, purified as previously described (7, 9), and stored at −80 °C in buffer A (20 mM Tris-HCl, pH 7.5, 200 mM KCl, 1.0 mM dithiothreitol, 1.0 mM EGTA). Full-length Ure2p assembly into fibrils was achieved by incubating the protein (50–100 μM) at 8 °C without shaking in buffer A for 48–96 h. Ure2p aggregates were examined by transmission electron microscopy, following negative staining with 1.0% uranyl acetate on carbon-coated grids (200-mesh) in a Philips EM 410 electron microscope. Ure2p oligomers were obtained soon after thawing the protein stored at −80 °C, whereas the heat-treated amyloid-like fibrils arose upon incubation of the native-like fibrils at 65 °C for 1 h. The covalent Ure2pC221 dimer was obtained by incubating the Ure2pC221 variant (50–100 μM) in buffer A without dithiothreitol in the presence of 3.0 mM H_2O_2. The excess of H_2O_2 was removed by dialysis against buffer A.

Cell Culture and Cell Viability Assay—Murine endothelioma H-END cells were kindly provided by Prof. F. Bussolino (University of Turin, Italy) and cultured in Dulbecco's modified Eagle's medium containing 10% fetal bovine serum, 3.0 mM glutamine, 100 units/ml penicillin, and 100 μg/ml streptomycin. All materials used for cell culture were from Sigma. The toxicity of the different forms of Ure2p aggregates was assessed by the 3-(4,5-dimethylthiazol-2-yl)-2,5-diphenyltetrazolium bromide (MTT) reduction inhibition test (25), as previously reported for aggregates of a different protein (26). In all of the experiments described in this paper, controls were performed by supplementing the cell cultures with identical volumes of buffer A for the same lengths of time.

Reactive Oxygen Species (ROS) Measurement—Intracellular ROS levels were determined using the fluorescent probe 5-(and-6)-chloromethyl-2′,7′-dichlorodihydrofluorescein diacetate, acetyl ester (CM-H_2 DCFDA) from Molecular Probes. Subconfluent H-END cells cultured on glass coverslips were incubated with 10.0 μM soluble Ure2p oligomers or native-like fibrils for either 1 or 5 h (aggregate concentrations are calculated as monomer protein concentration). After treatment, the cells were loaded with 5.0 μM CM-H_2 DCFDA for 20 min at 37 °C and then fixed with 2.0% buffered paraformaldehyde. CM-H_2 DCFDA fluorescence was detected at 488 nm using a confocal Bio-Rad MCR 1024 ES scanning microscope equipped with a krypton/argon laser source (15 milliwatts). The emitted fluorescence was collected with a Nikon Plan Apo ×60 oil immersion objective through a 510-nm-long wave pass filter. A series of at least 10 optical sections (512 × 512 pixels) was taken through the depth of the cells at 0.5-μm intervals and then projected as a single composite image by superimposition. Fluorescence quantification was performed by using National Institutes of Health ImageJ software (available on the World Wide Web at rsb.nih.gov/ij/).

Intracellular Free Ca^{2+} Levels—The cytosolic levels of free Ca^{2+} were measured using the fluorescent probe Fluo-3-acetoxymethyl ester from Molecular Probes. Briefly, subconfluent H-END cells cultured on glass coverslips were incubated at 37 °C for 5 min with 5.0 μM Fluo-3-acetoxymethyl ester prior to Ure2p addition. Then the cells were washed with serum-free Dulbecco's modified Eagle's medium without phenol red to remove the excess probe and mounted on the stage of the confocal microscope. Soluble Ure2p oligomers or native-like Ure2p fibrils (10.0 μM final concentration in serum-free Dulbecco's modified Eagle's medium without phenol red) were added to the cells, and Fluo-3 fluorescence was monitored at 488 nm 5 min after Ure2p addition (this time was supposed to be necessary for Ure2p aggregates to sediment and to interact with cells) using the software Time Course Kinetic (Bio-Rad). The same field was imaged every 20 s for 30 min. Fluorescence quantification was performed by ImageJ software.

Confocal Immunofluorescence—Cells grown on glass coverslips were treated for 4 h with the different forms of Ure2p aggregates (2.0 μM). After incubation, the cells were fixed in 2.0% buffered paraformaldehyde and counterstained with 50 μg/ml wheat germ agglutinin tetramethylrhodamine-conjugated (Molecular Probes) for 45 min at room temperature. Then the cells were permeabilized by treatment with acetone at −20 °C for 1 min and blocked with phosphate-buffered saline containing 0.5% bovine serum albumin and 0.2% glycerol. The cells were incubated overnight with rabbit polyclonal antibodies raised against full-length Ure2p diluted 1:2000 in the blocking solution. The immunoreaction was revealed with Alexa-488-conjugated anti-rabbit secondary antibodies (Molecular Probes) diluted 1:200 in phosphate-buffered saline. For inspection, the coverslips were mounted on the stage of the confocal microscope. The fluorescence was analyzed at 488- and 568-nm excitation for Alexa-488 and wheat germ agglutinin tetramethylrhodamine-conjugated, respectively. Observations were performed using a Nikon Plan Apo ×60 oil immersion objective. A series of at least

10 optical sections (512 × 512 pixels) was taken through the cells at intervals of 0.5 μm and projected as single composite image by superimposition. To eliminate out-of-focus light contribution, the images of Fig. 5 were deconvoluted using the three-dimensional deconvolution plugin (Biomedical Imaging Group, EPFL, Lausanne) of the Image J software.

DNA Fragmentation—Quantification of apoptosis was performed by the colorimetric TiterTACS™ 96-well apoptosis detection kit (R&D Systems Inc.). H-END cells were plated on 96-well plates at a density of 3000 cells/well in 100 μl of Dulbecco's modified Eagle's medium. After 48 h, the culture medium was exchanged with fresh medium containing full-length soluble Ure2p oligomers, native-like fibrils, or soluble Ure2p 94–354 (10.0 μM final concentrations). After 24 h, the cells were fixed in phosphate-buffered saline containing 3.7% formaldehyde and 10% sucrose. Labeling of DNA strand breaks was performed according to the manufacturer's instructions and quantified by measuring sample extinction at 450 nm using an automatic plate reader (Bio-Rad).

Caspase 3 Activity Assay—Cells treated for 24 h with full-length soluble Ure2p oligomers, native-like fibrils, or soluble Ure2p 94–354 (10.0 μM final concentrations) were lysed in 20 mM Tris-HCl buffer, pH 7.4, containing 250 mM NaCl, 2.0 mM EDTA, 0.1% Triton X-100, 5.0 μg/ml aprotinin, 5.0 μg/ml leupeptin, 0.5 mM phenylmethylsulfonyl fluoride, 4.0 mM sodium vanadate, and 1.0 mM dithiothreitol. The total protein content was determined in the clarified lysates with the Bradford reagent. Caspase 3 activity was determined by incubating 50 μg of total proteins for 2 h at 37 °C in the presence of 50 μM *N*-acetyl-DEVD-7-amino-4-trifluoromethyl coumarin fluorogenic substrate (Biomol Research Laboratories Inc.) in 50 mM HEPES-KOH buffer, pH 7.0, 10% glycerol, 0.1% 3-[(3-cholamidopropyl)-dimethylammonium]-1-propane sulfonate, 2.0 mM EDTA, 10 mM dithiothreitol. The fluorescent aminofluorocoumarin formation was determined at 400-nm excitation and 505-nm emission. In order to determine nonspecific substrate degradation in the assay, total protein samples were preincubated for 15 min at 37 °C in the presence or in the absence of the specific caspase inhibitor (100 nM *N*-acetyl-DEVD-aldehyde) prior to substrate addition. As a positive control, cells were treated with 2.0 μM staurosporine for 5 h prior to lysis.

Lactate Dehydrogenase Release Assay—Lactate dehydrogenase release was measured in the culture medium of cells exposed for 24 or 48 h to Ure2p aggregates by the Promega CytoTox-ONE™ homogeneous membrane integrity assay according to the manufacturer's instructions.

RESULTS

Viability of Cells Exposed to Differing Ure2p Aggregates—Different forms of Ure2p aggregates were prepared as described under "Experimental Procedures." Soluble Ure2p oligomers and native-like fibrils were characterized by transmission electron microscopy following negative staining at differing times of fibrillization and prior to the addition to the cell medium. Fig. 1*A* shows a transmission electron microscopy image of the soluble Ure2p oligomers formed at early aggregation times (0–1 h); these oligomers are represented by structured spherical particles with an outer diameter of 18 nm on average. Fig. 1*B* reports a magnification of one of these particles showing a ring-shaped appearance. Indeed, the particles appear to be made of globular units organized around a central hole with a diameter of about 3.0 nm. The insoluble form of Ure2p obtained by incubating the protein for 48–96 h at 8 °C in buffer A (see under "Experimental Procedures") consists of 20-nm-wide fibrils displaying variable lengths (0.5–10 μm) (Fig. 1*C*).

We investigated the toxicity to H-END cells of these different aggregates, together with that of the heat-treated amyloid fibrils (18) and of

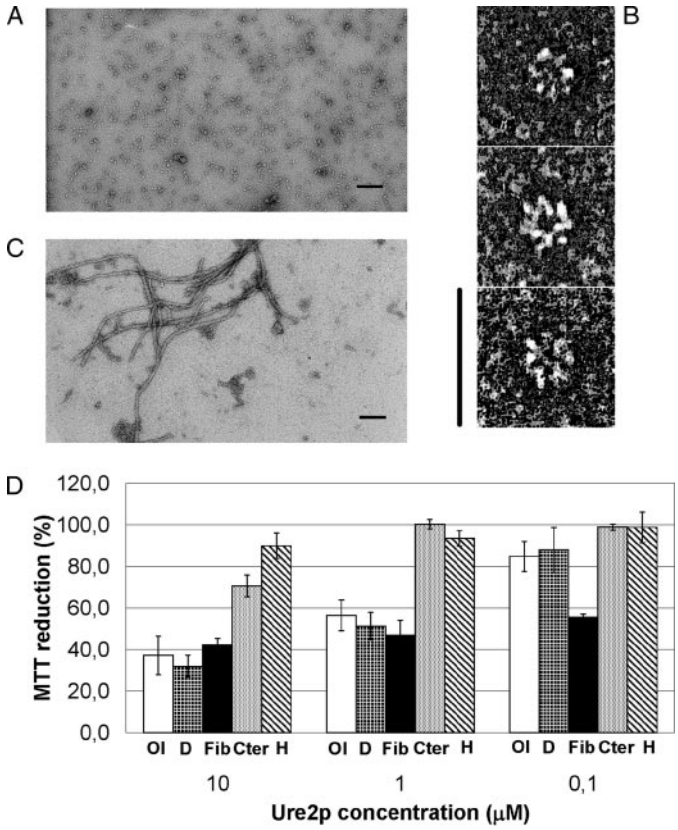

FIGURE 1. **Viability of H-END cells exposed to different molecular species of Ure2p measured by MTT assay.** *A–C*, negatively stained electron micrographs of the soluble Ure2p oligomers (*A*) and native-like fibrils (*C*) used throughout this study. *Bars* in *A* and *C*, 0.2 μm. Three ring-shaped soluble Ure2p oligomers are magnified in *B*. The associated *bar* represents 50 nm. *D*, viability of H-END cells exposed for 24 h to different molecular species of Ure2p at final concentrations of 10.0, 1.0, or 0.1 μM. Aggregate concentrations are calculated as monomer protein concentration. *Ol*, soluble Ure2p oligomers; *Fib*, native-like Ure2p fibrils; *Cter*, Ure2p 94–354; *H*, heat-treated Ure2p amyloid fibrils; *D*, Ure2pC221 covalent dimer. In this *graph*, cell viability is expressed as a percentage with respect to control cells treated with identical volumes of buffer A (for details, see "Experimental Procedures"). The values are mean ± S.D. obtained from five independent experiments carried out in triplicate.

the Ure2p covalent dimer that oligomerizes but is unable to form fibrils (16). In addition, the Ure2p 94–354 fragment (functional domain) able to bind GSH was used throughout this study to distinguish its contribution to the putative toxicity from that of the flexible N-domain. The cytotoxicity of Ure2p aggregates was evaluated by the MTT assay. A toxic effect was made evident by exposing the cells for 24 h to increasing concentrations (0.1, 1.0, and 10.0 μM) of soluble Ure2p oligomers or native-like fibrils or of the Ure2pC221 covalent dimer (Fig. 1*D*). Instead, heat-treated amyloid-like fibrils did not exhibit evident cytotoxicity even at the highest concentration tested (10.0 μM) (Fig. 1*D*), in agreement with the large body of data indicating that mature amyloid fibrils are substantially noncytotoxic (reviewed in Ref. 27). The toxic effect of 10.0 μM Ure2p oligomers and native-like fibrils was detectable as early as 3 h following the addition of the aggregates to the culture medium (Fig. 2*A*). We did not investigate earlier times. Native-like Ure2p fibrils displayed the highest toxicity, since the latter was detected at the lowest concentration used (0.1 μM), where oligomeric Ure2p or Ure2pC221 covalent dimer apparently were not toxic. We also measured cell viability upon the addition of soluble Ure2p oligomers or native-like fibrils in the 0.01–0.1 μM concentration range, and we found that 0.03 μM native-like fibrils were still significantly toxic (20% inhibition of MTT reduction), whereas under these conditions, the soluble oligomers did not display a measurable toxicity (Fig. 2*B*).

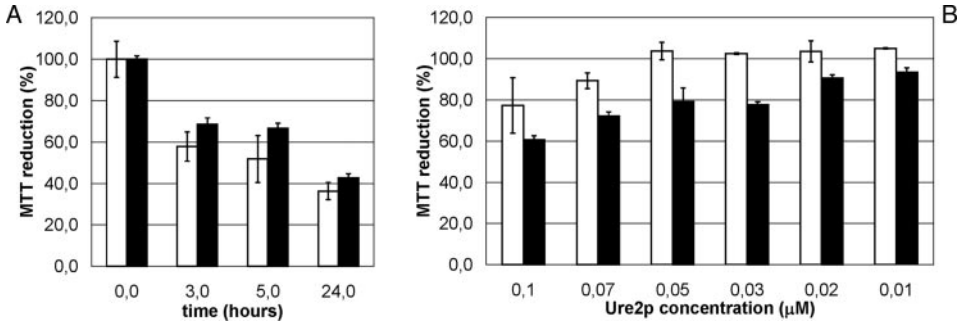

FIGURE 2. **Time and concentration dependence of cell viability upon exposure to soluble Ure2p oligomers and native-like fibrils.** *A*, H-END cells exposed for 3, 5, or 24 h to Ure2p oligomers (*empty bars*) and native-like fibrils (*filled bars*) at a final concentration of 10.0 μM. *B*, H-END cells exposed for 24 h to increasing concentrations (0.01–0.1 μM) of soluble Ure2p oligomers (*empty bars*) and native-like fibrils (*filled bars*). In both *graphs*, cell viability is expressed as percentage with respect to control cells treated with identical volumes of buffer A. The values are mean ± S.D. obtained from five independent experiments carried out in triplicate.

Native-like Ure2p oligomers and fibrils are toxic but still able to bind GSH, whereas the heat-treated fibrils are unable to bind GSH and are nontoxic. This prompted us to hypothesize that the oxidative stress (see below) resulting in cell injury by the toxic aggregates was merely a consequence of GSH depletion in exposed cells due to GSH binding by the aggregates rather than a direct effect of the aggregates themselves. To rule out this possibility, we investigated the toxicity of the functional C-terminal (residues 94–354) domain of Ure2p. The latter binds GSH and its analogues with an affinity identical to that of full-length Ure2p but is unable to form fibrils, since it lacks the prion domain needed for fibril assembly as well as for the propagation of the [URE3] phenotype in yeast cells. The data presented in Fig. 1*D* show that cells exposed to Ure2p 94–354 were only slightly impaired with respect to controls (25% inhibition of MTT reduction) at the highest concentration used (10.0 μM), and no significant toxicity was detected at lower concentrations. To confirm that Ure2p toxicity is not due to GSH binding and depletion, the GSH binding sites in the full-length Ure2p and in the Ure2p 94–354 were saturated with GSH upon incubation with equimolar amounts of the latter prior to the addition to the cell cultures. Under these conditions, no significant changes in the toxicity levels were observed (data not shown); we conclude from these observations that the strong toxicity associated with full-length Ure2p aggregates is not due to their GSH-binding properties.

Overall, from these observations we conclude that Ure2p toxicity is intimately associated with a toxic fold present in the native fibrils as well as in the oligomers but not in the amyloid-like fibrils generated heating the native-like fibrils. We further conclude that the observed toxicity is not due to changes in the intracellular redox environment of the exposed cells induced by direct binding and sequestering of GSH by native-like Ure2p molecules.

Redox Status and Intracellular Ca^{2+} Levels in Cells Exposed to Ure2p Aggregates—We have investigated the mechanism of cell damage in cells exposed to the toxic Ure2p aggregates by measuring the ROS and the intracellular free Ca^{2+} levels using the fluorescent probes CM-H_2 DCFDA and Fluo-3-acetoxymethyl ester, respectively. Intracellular ROS levels arose as early as 1 h after supplementing the cell culture medium with the soluble oligomers and native-like fibrils of Ure2p, reaching a 2-fold increase within 5 h (Fig. 3); such an increase was concomitant with the reduced cell viability observed by the MTT assay (Fig. 2*A*). The extents of ROS increase in cells exposed for 5 h to Ure2p oligomers or native-like fibrils were comparable. However, ROS increase was significantly faster when cells were exposed to soluble Ure2p oligomers (Fig. 3*C*). This could arise from a more rapid interaction of the Ure2p oligomers with the cell membrane, possibly due to their higher diffusion rate in the culture medium or to their ability to penetrate into the cells (see below).

A kinetic and quantitative analysis of the free Ca^{2+} levels in cells exposed to the Ure2p oligomers or native-like fibrils is shown in Fig. 4. The maximum fluorescence intensity (6-fold increase) was reached 9

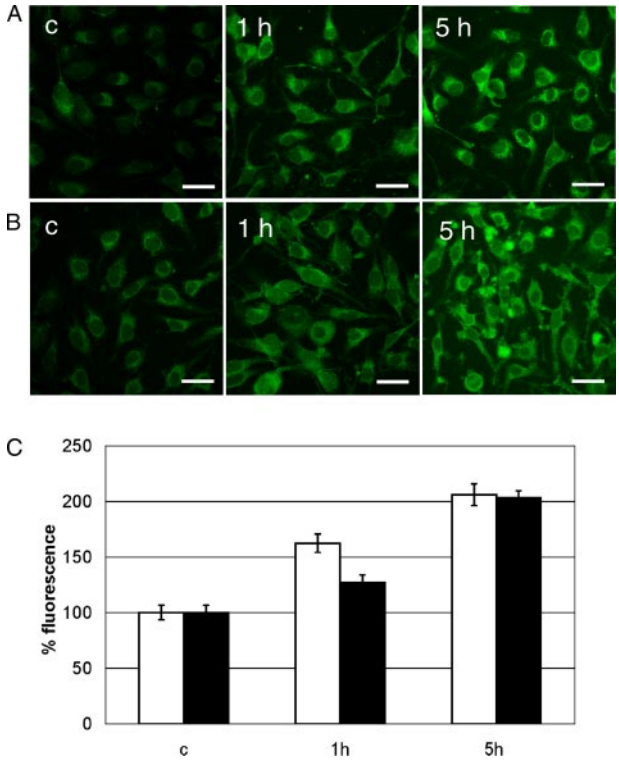

FIGURE 3. **Ure2p toxic aggregates induce oxidative stress in H-END cells.** *A* and *B*, confocal microscopy images of the redox status of H-END cells exposed for 1 or 5 h to 10.0 μM soluble Ure2p oligomers (*A*) or to 10.0 μM native-like Ure2p fibrils (*B*) prior to incubation with the fluorescent probe CM-H_2 DCFDA. Aggregate concentrations are calculated as monomer protein concentration. Control cells were treated for 5 h with the same volume of buffer A (see "Experimental Procedures"). The *bar* in *A* and *B* represents 30 μm. *C*, ROS levels in exposed cells. *Empty bars*, soluble Ure2p oligomers; *solid bars*, native-like Ure2p fibrils. The values are mean ± S.D. of the fluorescence measured in 30 different cellular areas (10 μm^2 each), selected from three distinct fields of the confocal microscope (10 areas/field).

min after supplementing the cell culture medium with soluble Ure2p oligomers. Fluorescence intensity decreased later but remained significantly higher than in control cells (Fig. 4, *A* and *B*). A similar, although less pronounced, increase in intracellular free Ca^{2+} concentration was observed in cells exposed to Ure2p native-like fibrils. However, in this case, the time course and the extent of the increase in fluorescence were significantly different from those observed upon the addition of comparable amounts of soluble Ure2p oligomers (Fig. 4*B*). The maximum fluorescence intensity was lower (3.5-fold increase) and was reached later (at 17 min). Interestingly, however, in cells exposed for 1 and 5 h to the soluble oligomeric or native-like fibrillar Ure2p, the intracellular Ca^{2+} levels dropped to the control values (data not shown), thus confirming the trend shown at earlier times by confocal microscopy. The increase of the intracellular free Ca^{2+} concentration could result from a destabilization of the membrane structure upon interaction with the

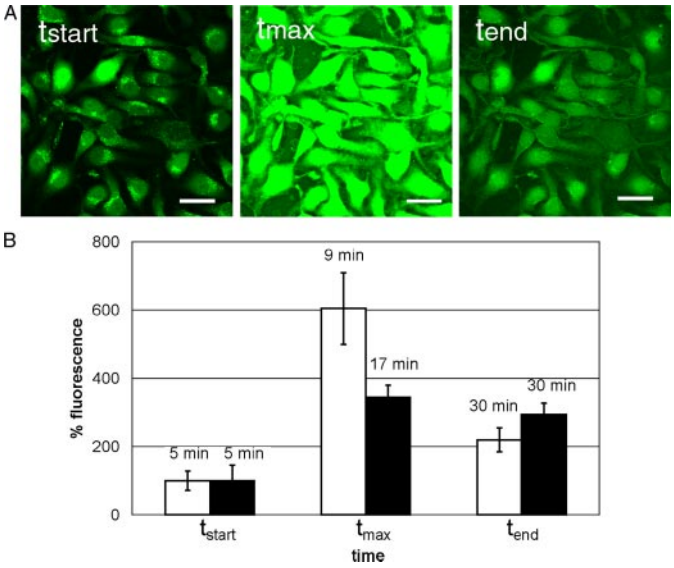

FIGURE 4. **Ure2p toxic aggregates induce changes in the intracellular free Ca^{2+} levels in H-END cells.** *A*, confocal microscopy imaging of intracellular free Ca^{2+} levels in H-END cells exposed to 10.0 μM soluble Ure2p oligomers. Aggregate concentrations are calculated as monomer protein concentration. These images show three different stages of the time course of intracellular Ca^{2+} changes measured continuously during the first 30 min of cell exposure to Ure2p oligomers. From *left* to *right*, t_{start} corresponds to start-up of the observations 5 min following Ure2p addition (see "Experimental Procedures"); t_{max} (9 min) is the time of the maximum fluorescence observed; t_{end} (30 min) is the fluorescence at the end of the observations. The *bar* represents 30 μm. *B*, quantitative analysis of the intracellular Ca^{2+} levels in H-END cells exposed to 10.0 μM soluble Ure2p oligomers (*empty bars*) or native-like fibrils (*filled bars*). The values are mean ± S.D. of the fluorescence measured in 10 different cell areas (10 μm^2 each) selected from the field of the confocal microscope.

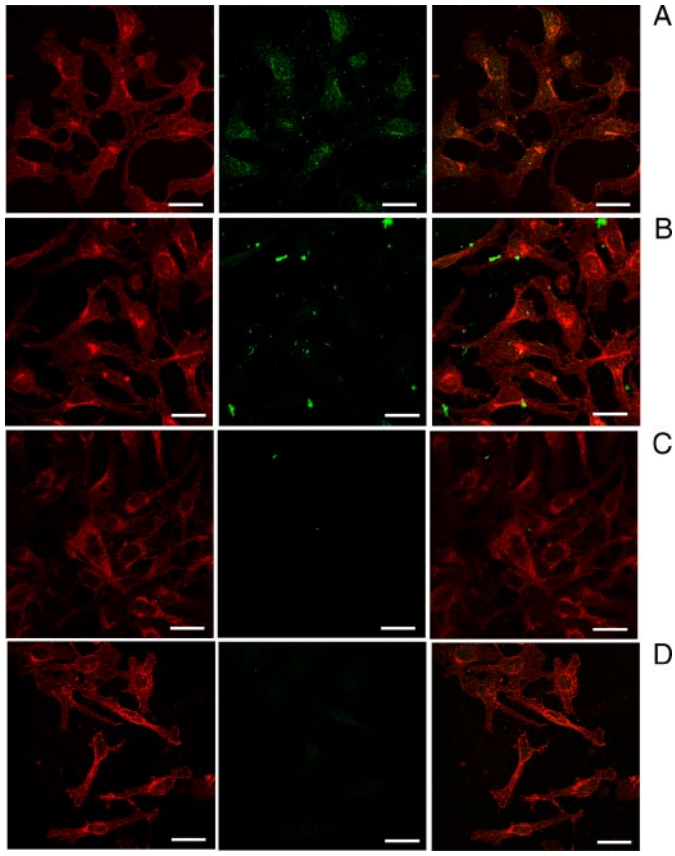

FIGURE 5. **Only the soluble Ure2p oligomers and the native-like fibrils bind to the plasma membrane.** H-END cells were exposed for 4 h to 2.0 μM soluble Ure2p oligomers (*A*), native-like fibrils (*B*), or heat-treated fibrils (*C*); aggregate concentrations are calculated as monomer protein concentration. Untreated cells (*D*) were incubated for 4 h with identical volumes of buffer A. *Left panels*, the cells were stained using wheat germ agglutinin tetramethylrhodamine-conjugated (*red*); *middle panels*, the different forms of Ure2p aggregates were revealed with Alexa-488-conjugated anti-rabbit secondary antibodies (*green*); *right panels*, merged images. Ure2p co-localization with membranes appears as *yellow* fluorescence. The *bar* represents 30 μm.

aggregates, and, in the case of the soluble oligomers, it could be a direct consequence of their pore-like shape. These observations suggest that, similarly to the toxic effects of protein aggregates of amyloid type, Ure2p toxicity is also associated with alterations of the intracellular free Ca^{2+} concentration, probably due to changes in membrane permeability and subsequent oxidative stress. This view is further supported by the data on Ure2p aggregate interaction with the plasma membrane and oligomer penetration inside cells (see below). Overall, these data indicate that soluble Ure2p oligomers possess higher efficiency than the native-like fibrils in promoting these changes in exposed cells.

Immunolocalization of Ure2p Oligomers and Native-like Fibrils—To assess whether oligomeric or native-like fibrillar Ure2p added to the culture medium was able to interact with and to cross the plasma membrane of H-END cells, we investigated the presence on the plasma membrane or inside the cells of the different forms of Ure2p used in this study. The experiments were carried out by confocal microscopy analysis using a polyclonal antibody raised against recombinant Ure2p. The soluble Ure2p oligomers (Fig. 5*A*) and, to a lesser extent, the native-like fibrils (Fig. 5*B*) were able to adsorb to the plasma membranes of cells exposed for 4 h. These data are consistent with the higher efficiency of the soluble oligomers in increasing the free Ca^{2+} level inside cells and hence in permeabilizing the cell membrane.

A careful analysis of the optical sections through the depth of the cells revealed the presence of immunopositive particles inside the cells exposed to the soluble oligomers (Fig. 6, *A–C*), whereas immunopositivity was not found inside cells exposed to native-like fibrils but only at the cell surface (Fig. 6, *D* and *E*), as could be expected with such large assemblies. Interestingly, heat-treated amyloid-like fibrils were never observed in cells nor associated with the cell membrane (Fig. 5*C*), suggesting that the surface of the amyloid-like Ure2p fibrils is not as "sticky" as that of the soluble oligomers or the native-like fibrils and does not interact with the cell surface. This finding supports the view that the tertiary and quaternary structure of Ure2p molecules within native-like fibrils are very different from those of the molecules found within amyloid-like fibrils. It is believed that, contrary to the prefibrillar aggregates, amyloid fibrils are stable end products of the aggregation process that do not interact easily with cell components, such as membranes, nor penetrate inside cells. Indeed, mature amyloid fibrils are often found to be remarkably inert, for example in their resistance to proteolysis and degradation (28), although recent findings support a dynamic equilibrium between fibrils and their constituent monomers (29).

Overall, our findings suggest that the impairment of cell viability following exposure to the soluble Ure2p oligomers or to the native-like fibrils is triggered by the interaction of these assemblies with the cell membrane and does not require their translocation inside the cells.

Apoptotic and Necrotic Markers—We quantified apoptotic cells in the population of cells exposed for 24 h to 10.0 μM Ure2p native-like aggregates by colorimetric detection of DNA fragmentation. Fig. 7*A* shows a 30% increase of DNA fragmentation in cells exposed to the soluble Ure2p oligomers or to the native-like fibrils as compared with untreated cells, whereas no significant increase in DNA fragmentation occurred in cells treated with the C-terminal domain (Ure2p 94–354). Moreover, a similar significant activation of the effector caspase 3 with respect to untreated cells could be observed in cells exposed for 24 h to Ure2p oligomers or native-like fibrils (Fig. 7*B*). No significant differ-

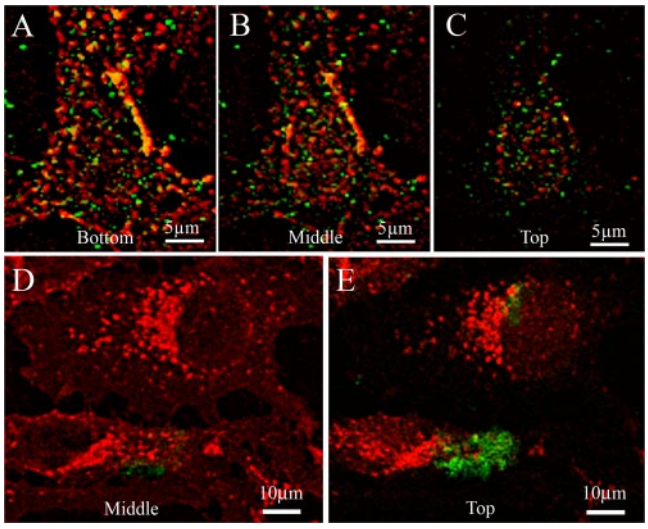

FIGURE 6. **Only the soluble Ure2p oligomers are able to penetrate into H-END cells.** Higher magnification view of cells shown in Fig. 5. *A–C*, H-END cells exposed for 4 h to soluble Ure2p oligomers. *D* and *E*, H-END cells exposed for 4 h to Ure2p native-like fibrils. *A–C*, three different optical sections through the depth of a single cell; the *yellow staining* after merging indicates that some of the aggregates are present within the cell. *Bars* in *A–C*, 5 μm. *D* and *E*, two different optical sections through the depth of the cells; note that Ure2p native-like fibrils are present only at the cell membrane. *Bars* in *D* and *E*, 10 μm.

ences in lactate dehydrogenase release were detected in treated and untreated cells even after 48-h exposure to the toxic Ure2p aggregates (Fig. 7*C*), suggesting that membrane integrity of the exposed H-END cells is not heavily affected under the experimental conditions used. These data indicate that the biochemical modifications occurring in cells exposed to the Ure2p toxic forms trigger the apoptotic pathway, eventually leading to cell death by apoptosis rather than by necrosis.

DISCUSSION

The data described in this paper show for the first time that native-like Ure2p aggregates are toxic to mammalian cultured cells. Interestingly, toxicity is associated with soluble oligomers, native-like nonamyloid fibrils, and the Ure2pC221 covalent dimer; in contrast, the heat-treated amyloid-like fibrils appear substantially nontoxic, as it has previously been reported for mature amyloid fibrils of most peptides and proteins (30, 31, 26). Finally, the Ure2p C-terminal domain, lacking the N-terminal segment necessary for aggregation but still able to bind GSH, is not cytotoxic. This finding strongly supports the idea that, besides aggregation, even Ure2p toxicity depends on the structural properties of the flexible N-terminal prion domain rather than on the GSH binding properties of the C-terminal functional domain. Our findings also indicate that native-like Ure2p fibrils retain a higher toxic potential upon dilution as compared with the soluble oligomers or with the Ure2pC221 covalent dimer. This finding could appear surprising, considering that the soluble forms of Ure2p can more easily reach cell membranes because of their higher diffusion rate in the cell culture medium. However, if we assume that Ure2p toxicity is the consequence of the interaction of Ure2p assemblies with the plasma membrane, it is conceivable that the injury caused to the cell membrane by native-like fibrils is more serious because of their size and therefore has a higher impact on cell survival than that caused by soluble Ure2p oligomers that, upon dilution, could not reach a density of binding to the cell membranes sufficient to cause remarkable membrane damage.

Several reports suggest that the impairment of cell viability, eventually leading to apoptosis or secondary necrosis, can be produced not only by amyloid aggregates formed by different peptides or proteins (32–34), but also by misfolded or unfolded systems devoid of amyloid

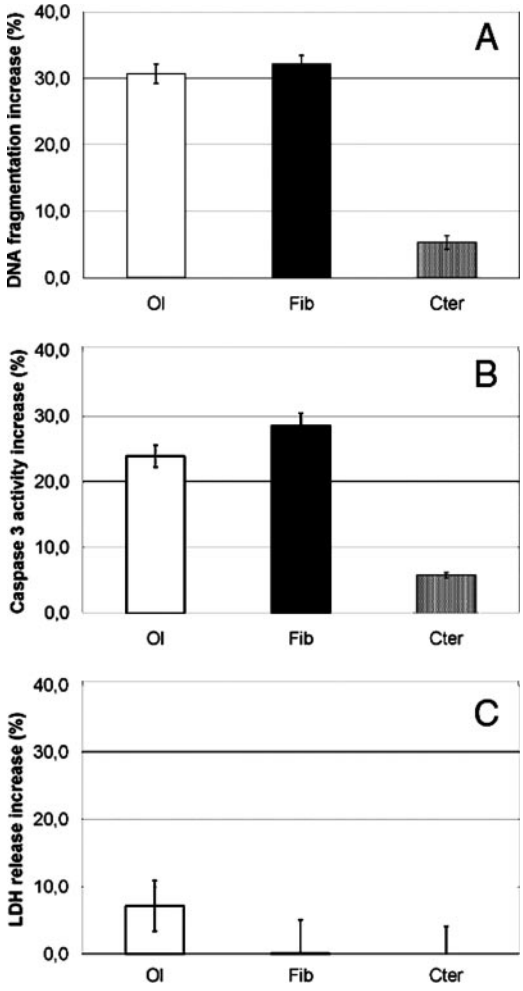

FIGURE 7. **Native-like Ure2p oligomers and fibrils induce apoptosis in H-END cells.** DNA fragmentation (*A*), caspase-3 activity increase (*B*), and lactate dehydrogenase release (*C*) were measured in H-END cells exposed to different molecular species of Ure2p. The increase in the proportion of these three parameters is expressed as a fraction of that observed in cells treated with identical volumes of buffer A. *Ol*, soluble Ure2p oligomers; *Fib*, native-like Ure2p fibrils; *Cter*, Ure2p 94–354. These values were obtained from one experiment of five independent measurements carried out in triplicate and yielding qualitatively identical results.

features. For example, it is known that an α-lactalbumin folding variant with molten globule features is able to kill specifically tumoral cells (35); similarly, apoptin multimers, exposing extensive hydrophobic surfaces (36), kill specifically tumoral cells (37). Endostatin also displays antitumoral specificity upon aggregation triggered by its interaction with membrane phosphatidylserine (38), whereas the 32-kDa ectodomain fragment of CD44 displays selective toxicity to differing cell lines (39). Most pore-forming toxins of bacterial or eukaryotic origin kill target cells by oligomerizing into their plasma membranes, where they produce nonspecific pores (40–42). Finally, several peptides and proteins have been shown to form doughnut-shaped prefibrillar assemblies before further organizing into mature amyloid fibrils (43–47).

These and other data suggest that the toxicity associated to the monomeric, oligomeric, or polymeric forms of a wide variety of polypeptides either endowed with classical amyloid features or not may come from biochemical modifications of membrane permeability and subsequent oxidative stress (48, 49). They also suggest that such an interaction is favored by the presence, in these species, of suitable (*i.e.* most often hydrophobic) surfaces as well as of a suitable membrane lipid composition in exposed cells. Indeed, it has been repeatedly reported

that anionic phospholipids, such as phosphatidylserine, which becomes exposed in the outer membrane leaflet in apoptotic and tumoral cells, are putative docking sites for amyloid aggregates or can favor aggregate formation, thus initiating membrane impairment (38, 50, 51). Membrane cholesterol modulates membrane fluidity and may affect the incorporation of toxic aggregates into exposed cells (24, 52) as well as membrane-associated Abeta fibrillogenesis and toxicity in neuronal cells (53, 54).

Calcium dysregulation and membrane disruption have been proposed as ubiquitous neurotoxic mechanisms of toxicity of soluble amyloid oligomers (55). Indeed, in most cases, amyloid cytotoxicity requires the binding of the aggregate to the plasma membrane with subsequent membrane destabilization, loss of ion-specific permeability, and oxidative stress (56–62).

The findings we report here on the toxicity of soluble Ure2p oligomers and native-like fibrils are consistent with the above mentioned scenario. Indeed, we observed a burst in the intracellular free Ca^{2+} concentration at 9/17 min after cell exposure to the Ure2p toxic species, followed by a progressive reduction at later times, whereas ROS increase was sustained for longer time periods. These observations suggest that, in our model, oxidative stress is a secondary event, given that the increase of intracellular ROS levels occurs only at later stages of treatment, whereas no alterations in redox status can be observed during the first 30 min of exposure (data not shown). Further evidence supporting the idea that the mechanism of cell damage is triggered at the plasma membrane level comes from the observation that Ure2p oligomers and native-like fibrils stick to the plasma membrane of H-END cells more efficiently than the heat-treated amyloid fibrils, as shown in Fig. 5. After binding to the membranes, Ure2p oligomers are internalized. We have not investigated whether oligomer internalization requires an endocytosis-like mechanism; however, this finding supports strongly the ability of Ure2p oligomers to cross the plasma membrane and to penetrate into cells similarly to prefibrillar aggregates of a number of proteins (62–64). The soluble oligomers of Ure2p possess a pore-like shape and could act in a manner similar to other peptides that compromise the integrity of cell membranes, generating nonspecific pores and disrupting their selective permeability. It is reasonable to envisage that the interaction of soluble and fibrillar Ure2p oligomers also impact membrane plasticity. However, our observations do not support such a scenario, since cells facing these oligomers maintain substantially the same shape, which is not what is expected if membrane plasticity were compromised. Moreover, the analysis of apoptotic and necrotic markers indicates that, as it has been shown for most cultured cells exposed to toxic amyloid aggregates, apoptosis, rather than necrosis, is the final outcome of the insult given by the toxic Ure2p forms to H-END cells.

In conclusion, toxicity appears as an intrinsic feature of Ure2p native-like aggregates, intimately associated with a shared toxic fold, driven by the N-terminal domain of Ure2p, and required for an efficient interaction with cell membranes, that is maintained upon dimerization and following protein assembly into soluble ring-shaped oligomers and native-like fibrils. This behavior differs somehow from what has been proposed for amyloids, where toxicity follows extensive molecular rearrangements and appears restricted mainly to amyloid prefibrillar aggregates (26, 65). Therefore, it is possible to generalize the toxicity of protein monomers, oligomers, or polymers, not necessarily of amyloid type, endowed with structural features (usually the exposure of hydrophobic patches), leading them to physically interact with and/or organize into cell membranes (typically the plasma membrane). The resulting physical destabilization of the membranes and modifications of their biochemical features would be at the origin of the chain of events leading to cell death.

REFERENCES

1. Prusiner, S. B. (1998) *Proc. Natl. Acad. Sci. U. S. A.* **95,** 13363–13383
2. Wickner, R. B. (1996) *Annu. Rev. Genet.* **30,** 109–139
3. Masison, D. C., and Wickner, R. B. (1995) *Science* **270,** 93–95
4. Edskes, H. K., Gray, V. T., and Wickner, R. B. (1999) *Proc. Natl. Acad. Sci. U. S. A.* **96,** 1498–1503
5. Magasanik, B. (1992) in *The Molecular and Cellular Biology of the Yeast Saccharomyces cerevisiae* (Jones, E. W., Pringle, J. R., and Broach, J. R., eds) Vol. 12, pp. 283–317, Cold Spring Harbor Laboratory Press, Plainview, NY
6. Blinder, D., Coschigano, P. W., and Magasanik, B. (1996) *J. Bacteriol.* **178,** 4734–4736
7. Thual, C., Bousset, L., Komar, A. A., Walter, S., Buchner, J., Cullin, C., and Melki, R. (2001) *Biochemistry* **40,** 1764–1773
8. Bousset, L., Redeker, V., Decottignies, P., Dubois, S., Le Marechal, P., and Melki, R. (2004) *Biochemistry* **43,** 5022–5032
9. Thual, C., Komar, A. A., Bousset, L., Fernandez-Bellot, E., Cullin, C., and Melki, R. (1999) *J. Biol. Chem.* **274,** 13666–13674
10. Bousset, L., Belrhali, H., Janin, J., Melki, R., and Morera, S. (2001) *Structure (Camb.)* **9,** 39–46
11. Umland, T. C., Taylor, K. L., Rhee, S., Wickner, R. B., and Davies, D. R. (2001) *Proc. Natl. Acad. Sci. U. S. A.* **98,** 1459–1464
12. Board, P. G., Coggan, M., Chelvanayagam, G., Easteal, S., Jermiin, L. S., Schulte, G. K., Danley, D. E., Hoth, L. R., Griffor, M. C., Kamath, A. V., Rosner, M. H., Chrunyk, B. A., Perregaux, D. E., Gabel, C. A., Geoghegan, K. F., and Pandit, J. (2000) *J. Biol. Chem.* **275,** 24798–24806
13. Bousset, L., Belrhali, H., Melki, R., and Morera, S. (2001) *Biochemistry* **40,** 13564–13573
14. Wickner, R. B., Taylor, K. L., Edskes, H. K., Maddelein, M. L., Moriyama, H., and Roberts, B. T. (2000) *J. Struct. Biol.* **130,** 310–322
15. Mihara, H., Takahashi, Y., and Ueno, A. (1998) *Biopolymers* **47,** 83–92
16. Bousset, L., Thomson, N. H., Radford, S. E., and Melki, R. (2002) *EMBO J.* **21,** 2903–2911
17. Taylor, K. L., Cheng, N., Williams, R. W., Steven, A. C., and Wickner, R. B. (1999) *Science* **283,** 1339–1343
18. Bousset, L., Briki, F., Doucet, J., and Melki, R. (2003) *J. Struct. Biol.* **141,** 132–142
19. Bai, M., Zhou, J. M., and Perrett, S. (2004) *J. Biol. Chem.* **279,** 50025–50030
20. Baxa, U., Taylor, K. L., Wall, J. S., Simon, M. N., Cheng, N., Wickner, R. B., and Steven, A. C. (2003) *J. Biol. Chem.* **278,** 43717–43727
21. Kajava, A. V., Baxa, U., Wickner, R. B., and Steven, A. C. (2004) *Proc. Natl. Acad. Sci. U. S. A.* **101,** 7885–7890
22. Baxa, U., Ross, P. D., Wicknerand, R. B., and Steven, A. C. (2004) *J. Mol. Biol.* **339,** 259–264
23. Bucciantini, M., Rigacci, S., Berti, A., Pieri, L., Cecchi, C., Nosi, D., Formigli, L., Chiti, F., and Stefani, M. (2005) *FASEB J.* **19,** 437–439
24. Cecchi, C., Baglioni, S., Fiorillo, C., Pensalfini, A., Liguri, G., Nosi, D., Rigacci, S., Bucciantini, M., and Stefani, M. (2005) *J. Cell Sci.* **118,** 3459–3470
25. Abe, K., and Kimura, H. (1996) *J. Neurochem.* **67,** 2074–2078
26. Bucciantini, M., Giannoni, E., Chiti, F., Baroni, F., Formigli, L., Zurdo, J., Taddei, N., Ramponi, G., Dobson, C. M., and Stefani, M. (2002) *Nature* **416,** 507–511
27. Stefani, M., and Dobson, C. M. (2003) *J. Mol. Med.* **81,** 678–699
28. Zurdo, J., Guijarro, J. I., and Dobson, C. M. (2001) *J. Am. Chem. Soc.* **125,** 8141–8142
29. Carulla, N., Caddy, G. L., Hall, D. R., Zurdo, J., Gairi, M., Feliz, M., Giralt, E., Robinson, C. V., and Dobson, C. M. (2005) *Nature* **436,** 554–558
30. Hardy, J., and Selkoe, D. J. (2002) *Science* **297,** 353–356
31. Kayed, R., Head, E., Thompson, J. L., McIntire, T. M., Milton, S. C., Cotman, C. W., and Glabe, C. G. (2003) *Science* **300,** 486–489
32. Zhang, Y., McLaughlin, R., Goodyer, C., and LeBlanc, A. (2002) *J. Cell Biol.* **156,** 519–529
33. Morishima, Y., Gotoh, Y., Zieg, J., Barrett, T., Takano, H., Flavell, R., Davis, R. J., Shirasaki, Y., and Greenberg, M. E. (2001) *J. Neurosci.* **21,** 7551–7560
34. Orrenius, S., Zhivotovsky, B., and Nicotera, P. (2003) *Nat. Rev. Mol. Cell. Biol.* **4,** 552–565
35. Svanborg, C., Agerstam, H., Aronson, A., Bjerkvig, R., Duringer, C., Fischer, W., Gustafsson, L., Hallgren, O., Leijonhuvud, I., Linse, S., Mossberg, A. K., Nilsson, H., Pettersson, J., and Svensson, M. (2003) *Adv. Cancer Res.* **88,** 1–29
36. Leliveld, S., Noteborn, M. H., and Abrahams, J. P. (2003) *Eur. J. Biochem.* **270,** 3619–3627
37. Zhang, Y. H., Leliveld, S. R., Kooistra, K., Molenaar, C., Rohn, J. L., Tanke, H. J., Abrahamas, J. P., and Noteborn, M. H. (2003) *Exp. Cell Res.* **289,** 36–46
38. Zhao, H., Jutila, A., Nurminen, T., Wickström, S. A., Keski-Oja, J., and Kinnunen, P. K. J. (2005) *Biochemistry* **44,** 2857–2863
39. Choi, J., Miller, A. M., Nolan, M. J., Yue, B. Y., Thotz, S. T., Clark, A. F., Agarwal, N., and Knepper, P. A. (2005) *Invest. Ophthalmol. Vis. Sci.* **46,** 214–222

40. Hotze, E. M., Heuck, A. P., Czajkowsky, M., Shao, Z., Johnson, A. E., and Tweten, R. K. (2002) *J. Biol. Chem.* **277,** 11597–11605
41. Valeva, A., Schnabell, R., Valevi, I., Boukhallouk, F., Bhakdi, S., and Palmer, M. (2001) *J. Biol. Chem.* **276,** 14835–14841
42. Miyata, S., Matsushita, O., Minami, J., Katayama, S., Shimamoto, S., and Okabe, A. (2001) *J. Biol. Chem.* **276,** 13778–13783
43. Sousa, M. M., Cardoso, I., Fernandes, R., Guimaraes, A., and Saraiva, M. J. (2001) *Am. J. Pathol.* **159,** 1993–2000
44. Hirakura, Y., and Kagan, B. L. (2001) *Amyloid* **8,** 94–100
45. Lin, H., Bhatia, R., and Lal, R. (2001) *FASEB J.* **15,** 2433–2444
46. Lashuel, H. A., Hartley, D., Petre, B. M., Walz, T., and Lansbury, P. T. (2002) *Nature* **418,** 291
47. Wang, L., Lashuel, H. A., Walz, T., and Colon, W. (2002) *Proc. Natl. Acad. Sci. U. S. A.* **99,** 15947–15952
48. Kourie, J. I., and Henry, C. L. (2002) *Clin. Exp. Pharmacol. Physiol.* **29,** 741–753
49. Kagan, B., Azimov, R., and Azimova, R. (2004) *J. Membr. Biol.* **202,** 1–10
50. Zhao, H., Tuominen, E. K. J., and Kinnunen, P. K. J. (2004) *Biochemistry* **43,** 10302–10307
51. Lee, G., Pollard, H. B., and Arispe, N. (2002) *Peptides* **23,** 1249–1263
52. Arispe, N., and Doh, M. (2002) *FASEB J.* **16,** 1526–1536
53. Yip, C. M., Elton, E. A., Darabie, A. A., Morrison, M. R., and McLaurin, J. (2001) *J. Mol. Biol.* **311,** 723–734
54. Ji, S. R., Wu, Y., and Sui, S. F. (2002) *J. Biol. Chem.* **277,** 6273–6279
55. Demuro, A., Mina, E., Kayed, R., Milton, S. C., Parker, I., and Glabe, C. G. (2005) *J. Biol. Chem.* **280,** 17294–17300
56. Mattson, M. P. (1999) *Methods Enzymol.* **309,** 733–768
57. Kanski, J., Varadarajan, S., Aksenova, M., and Butterfield, D. A. (2001) *Biochim. Biophys. Acta* **1586,** 190–198
58. Junn, E., and Mouradian, M. M. (2002) *Neurosci. Lett.* **320,** 146–150
59. Wyttenbach, A., Sauvageot, O., Carmichael, J., Diaz-Latoud, C., Arrigo, A. P., and Rubinsztein, D. C. (2002) *Hum. Mol. Genet.* **11,** 1137–1151
60. Kawahara, M., Kuroda, Y., Arispe, N., and Rojas, E. (2000) *J. Biol. Chem.* **275,** 14077–14083
61. Milhavet, O., and Lehmann, S. (2002) *Brain Res. Brain Res. Rev.* **38,** 328–339
62. Bucciantini, M., Calloni, G., Chiti, F., Formigli, L., Nosi, D., Dobson, C. M., and Stefani, M. (2004) *J. Biol. Chem.* **279,** 31374–31382
63. Yang, W., Dunlap, J. R., Andrews, R. B., and Wetzel, R. (2002) *Hum. Mol. Genet.* **11,** 2905–2917
64. Kranenburg, O., Kroon-Batenburg, L. M. J., Reijerkerk, A., Wu, Y. P., Voest, E. E., and Gebbink, M. F. (2003) *FEBS Lett.* **539,** 149–155
65. Kayed, R., Sokolov, Y., Edmonds, B., McIntire, T. M., Milton, S. C., Hall, J. E., and Glabe, C. G. (2004) *J. Biol. Chem.* **279,** 46363–46366

The Yeast Prion Ure2p Native-like Assemblies Are Toxic to Mammalian Cells Regardless of Their Aggregation State

Laura Pieri, Monica Bucciantini, Daniele Nosi, Lucia Formigli, Jimmy Savistchenko, Ronald Melki and Massimo Stefani

J. Biol. Chem. 2006, 281:15337-15344.
doi: 10.1074/jbc.M511647200 originally published online March 29, 2006
